

# A Possible Site of Cosmic Ray Acceleration in the Supernova Remnant IC 443

Jonathan W. Keohane<sup>1</sup>, R. Petre<sup>2</sup>, Eric V. Gotthelf<sup>3</sup>

*The Laboratory for High Energy Astrophysics  
Code 662, NASA/GSFC, Greenbelt, MD 20771*

M. Ozaki, K. Koyama

*Department of Physics, Faculty of Science  
Kyoto University, Sakyo-ku, Kyoto 606-01, Japan*

February 5, 1997

Accepted by *The Astrophysical Journal*

## ABSTRACT

We present evidence for shock acceleration of cosmic rays to high energies ( $\sim 10$  TeV) in the supernova remnant IC 443. X-ray imaging spectroscopy with *ASCA* reveals two regions of particularly hard emission: an unresolved source embedded in an extended emission region, and a ridge of emission coincident with the southeastern rim. Both features are located on part of the radio shell where the shock wave is interacting with molecular gas, and together they account for a majority of the emission at 7 keV. Though we would not have noticed it *a priori*, the unresolved feature is coincident with one resolved by the *ROSAT* HRI. Because this feature overlaps a unique region of flat radio spectral index ( $\alpha < 0.24$ ), has about equal light-crossing and synchrotron loss times, and a power law spectrum with a spectral index of  $\alpha=1.3\pm0.2$ , we conclude that the hard X-ray feature is synchrotron radiation from a site of enhanced particle acceleration. Evidence against a plerion includes a lack of observed periodicity (the pulsed fraction upper limit is 33%), the spectral similarity with the more extended hard region, the location of the source outside the 95% error circle of the nearby *EGRET* source, the fact that it is nestled in a bend in the molecular cloud ring with which IC 443 is interacting, and the requirement of an extremely high transverse velocity ( $\geq 5,000$  km/s). We conclude that the anomalous feature is most likely tracing enhanced particle acceleration by shocks that are formed as the supernova blast wave impacts the ring of molecular clouds.

*Subject headings:* acceleration of particles — radiation mechanisms: non-thermal — shock waves — cosmic rays — supernova remnants — supernovae: individual (IC443)

<sup>1</sup>Astronomy Department, The University of Minnesota; E-mail: jonathan@lheamail.gsfc.nasa.gov

<sup>2</sup>E-mail: petre@lheavx.gsfc.nasa.gov

<sup>3</sup>Universities Space Research Association; E-mail: gotthelf@lheavx.gsfc.nasa.gov

## 1. Introduction

It is generally accepted from energy budget considerations that supernova remnants (SNRs) are the primary source of galactic cosmic rays (CRs), which are inferred to span the energy range from about  $10^8$  to  $10^{14}$  eV (Blandford & Ostriker 1978; Axford 1994; Biermann 1995, and references therein). Though radio observations of synchrotron radiation from supernova remnants supply bountiful evidence that they are the source of CRs at GeV energies, evidence regarding higher energy cosmic rays is largely circumstantial. A search for ultra-high energy  $\gamma$ -rays ( $\sim 10^{14}$  eV) coincident with SNRs detected nothing significant (Allen, et al. 1995). The best evidence thus far for shock acceleration of  $\sim 100$  TeV CRs, comes from X-ray observations of SN 1006 (Koyama et al. 1995). SN 1006 appears to be unique in that the non-thermal X-ray flux from its shell dominates the thermal, but current limits on the non-thermal flux from the shells of other young SNR do not exclude the presence of a synchrotron component, and hence ongoing CR acceleration to TeV energies.

In this paper we report the discovery of a site in another SNR in which high energy cosmic rays are possibly being accelerated, but by a different mechanism from that in SN 1006. Using *ASCA* GIS data, we have found a concentration of hard X-ray emission along the southern rim of the middle-aged remnant IC 443, whose spectrum is consistent with a power law, and whose morphology suggests enhanced shock acceleration resulting from the SNR shock encountering dense clouds in the ISM. The observations are consistent with the prediction of such an effect by Jones & Kang (1993, hereafter JK93).

IC 443 (G189.1+3.0) is a nearby ( $\approx 1.5$  kpc) supernova remnant (SNR) of intermediate age. Many infrared and radio line observations have demonstrated that IC 443 is interacting with a ring of molecular clouds (e.g., DeNoyer 1979; Burton *et al.* 1988, hereafter BGBW; Burton *et al.* 1990; Dickman *et al.* 1992, hereafter DSZH; van Dishoeck *et al.* 1993). The region in which the most complex interactions between the molecular cloud and the SNR shock is occurring also has an unusually flat radio spectral index for a shell-like SNR ( $\alpha < 0.24$  – Green 1986, hereafter G86).

In the X-ray band, IC 443 has been the subject of a number of comprehensive studies, most notably those of Petre *et al.* (1988, hereafter PSSW) and Asaoka & Aschenbach (1994, hereafter AA94). It has an irregu-

lar soft X-ray morphology, influenced strongly by its interactions with an H I cloud to the northeast and the foreground molecular cloud and shadowing by the foreground SNR G189.6+3.3. Using *Ginga*, Wang et al. (1992, hereafter WAHK) resolved spectrally a hard component which they were able to characterize by either a thermal model with  $kT \sim 14$  keV or a power law with photon index  $\Gamma \sim 2.2$ . Scanning observations by *HEAO1* A-2 showed that the hard emission is more centrally located than the bright soft emission. Neither the A-2 nor the *Ginga* observations provided information regarding the extent of the hard emission.

IC 443 is also coincident with a high energy  $\gamma$ -ray source, which has led to speculation that the  $\gamma$ -rays are produced by the interaction of cosmic rays, accelerated by IC 443's shocks, with nearby molecular cloud material (Sturner & Dermer 1995; Esposito *et al.* 1996, hereafter EHKS). Models of broad-band non-thermal spectra have recently been produced by Sturner et al. (1996); in these synchrotron radiation dominates from the radio to the soft X-ray, while electron bremsstrahlung and  $\pi^0$  decay dominate the  $\gamma$ -ray emission for a supernova remnant like IC 443.

Our paper is organized as follows. We first present the *ASCA* GIS images showing the location of the hard X-ray emission region (§2.1). We compare the *ASCA* image with that from the *ROSAT* HRI. We then discuss our analysis of the GIS spectrum and the GIS and HRI light curves from that region (§2.4). Finally, we discuss possible emission mechanisms and the implications for the acceleration of cosmic rays by supernova remnants (§3.2).

## 2. Observations and Analysis

Table 1: *ASCA* observations of the SNR IC 443

Sequence #	10011010	51023000
Mission Phase	PV phase	AO-1
RA (J2000)	06 <sup>h</sup> 17 <sup>m</sup> 25 <sup>s</sup>	06 <sup>h</sup> 16 <sup>m</sup> 19 <sup>s</sup>
Declination	+22°40'37"	+22°26'53"
GIS Exposure	20.2 ks	34.7 ks
Date	April 14, 1993	March 9, 1994

### 2.1. The *ASCA* GIS X-ray Maps

*ASCA* performed observations of two adjacent regions of IC 443, one during the Performance Verification (PV) phase of the mission, the other during the first cycle of guest observations (AO-1). The relevant

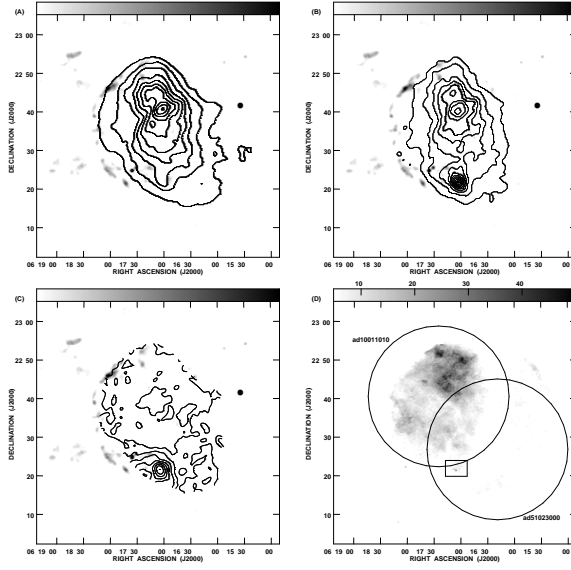


Fig. 1.— Soft (A) and hard (B) GIS contour images of IC 443. The energy bands are 1.1–2.1 and 2.1–12.0 keV respectively. The ratio of the two bands (C) is also shown (blanked in regions of low soft X-ray surface brightness). The contour levels in each figure are multiples of 10% of the peak. For reference, we have shown in grey-scale (A, B, C), a 1.4 GHz radio map from the VLA sky survey (10–100 mJy/beam). Image D shows our *ROSAT* HRI mosaic of IC 443; the GIS field of view for each observation and the region shown in Figure 4 are overlaid.

information about these observations is contained in Table 1. We extracted these data sets from the *ASCA* public archive. In figures 1 A and B, we show exposure-corrected GIS mosaic images for the hard (2.1–12 keV) and soft bands (1.1–2.1 keV). These appear highly correlated, except for a bright feature in the hard band map, centered at RA = 06<sup>h</sup>17<sup>m</sup>05<sup>s</sup>, Dec = +22°21'30" (J2000). The anomalous nature of this feature is shown in dramatic fashion in figure 1C, a spectral hardness ratio map, constructed by dividing the hard band map by the soft. There it can be seen that the other features, associated with the diffuse thermal emission in IC 443, all have similar spectral hardness, but the hard X-ray feature (HXF) stands out. The *ASCA* GIS brightness distribution within the hard feature is consistent with that expected from a source smaller than  $\sim 1'$ . The hard feature is  $\sim 12'$  off axis so it was not in the SIS field of view.

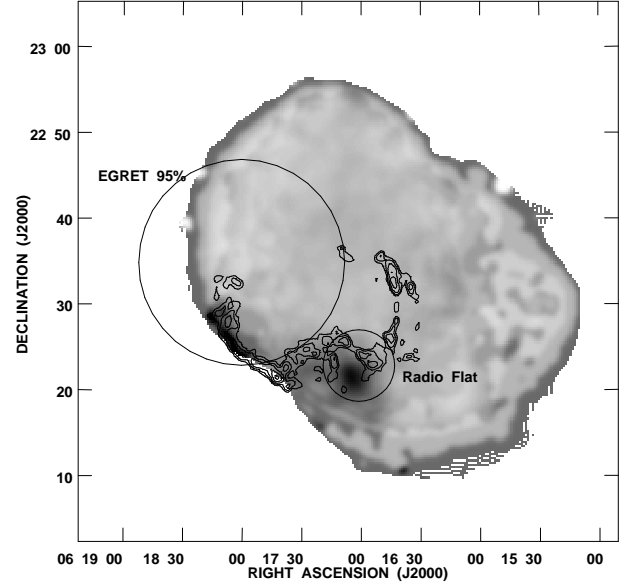


Fig. 2.— The *ASCA* GIS hardness ratio map ( $F_{2.1-12 \text{ keV}}/F_{1.1-2.1 \text{ keV}}$ ) is shown in grey-scale. The overlaid drawings are: the EGRET  $\gamma$ -ray detection circle (EHKS), the region of flat radio spectral index (G86) and a contour plot of the  $v=1-0S(1)$   $\text{H}_2$  emission line intensity (BGBW).

In addition, there is a ridge of spectral hardness located northeast of the HXF along the radio-bright rim of the remnant. This second feature is not shown in Fig. 1C because it was blanked due to its small soft X-ray count rate. It is shown, however, in Figs. 2 and 3. As will be discussed in more detail in §2.4, the hard flux from the observed portion of the ridge is about half the hard flux from the HXF and the two regions can account for a majority of the total hard *ASCA* flux.

## 2.2. *ROSAT* HRI Image

The region containing the HXF was observed for 30 ks using the *ROSAT* HRI as part of a program to create a complete high resolution X-ray image of IC 443. In Fig. 1D, we show the complete HRI mosaic, with the GIS fields of view overlaid. A surface brightness enhancement appears approximately at the location of the HXF. The HRI map of the region containing the HXF is shown in Fig. 4, with the GIS hardness ratio contours overlaid. The feature's central core has an angular extent of about  $10'' \times 5''$ , with extended lower level structure of about  $1'$  in extent. The elon-

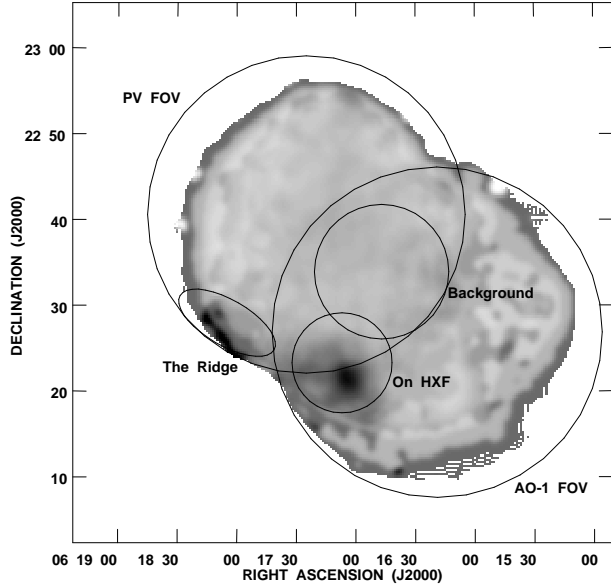


Fig. 3.— The regions where *ASCA* GIS data were selected for our spectral analysis and the approximate *ASCA* GIS fields of view, overlaid on the same hardness ratio map as shown in Fig. 2. We purposely chose a larger than needed region about the HXF and the ridge in order to spectrally distinguish between the thermal and non-thermal spectra.

gation of the central core is perpendicular to the orientation of the low level emission and does not resemble the HRI point spread function, so we believe it to be resolved.

### 2.3. Spatial Correlations with Other Bands

In Fig. 2 we overlay on the GIS spectral hardness ratio map possibly related spatial information from other bands: the EGRET 95 percent confidence error circle (EKHS), contours of H<sub>2</sub> emission (BGBW) which locate the sites of the most intense SNR shock/cloud interaction, and the region in which the  $\lambda\lambda 20-200$  cm spectral index is appreciably flatter than elsewhere in IC 443 (G86). The HXF is just outside a concave arc of H<sub>2</sub> emission, but correlates well with the region of flat radio index. Interestingly, it is well outside the EGRET error circle. In the Digitized Sky Survey (Lasker et al. 1990), there are some faint filaments in this region, but no obvious unresolved sources near the hard feature. A search of the

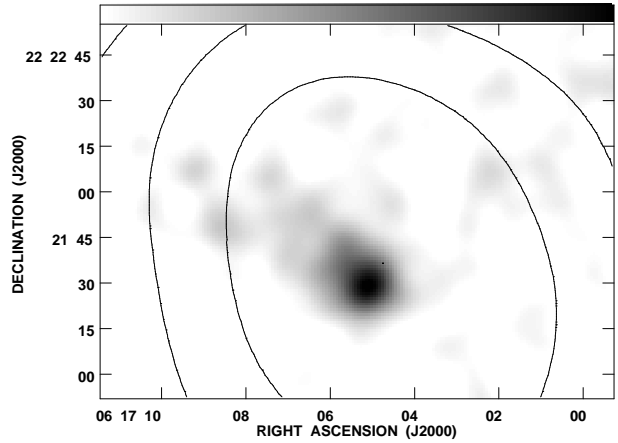


Fig. 4.— The 10'' FWHM Gaussian smoothed *ROSAT* HRI (grey-scale) and the 60'' resolution hardness *ASCA* hardness ratio map shown with the same contour levels as figure 1C. The grey-scale range is 10-45 counts per 10'' diameter circular “beam.”

most recent on-line pulsar catalog (Taylor et al. 1993) reveals none near the feature.

In addition to the main hard feature, the ridge of hard emission overlaps the H<sub>2</sub> emission region, but does not appear coincident with any region of radio spectral index flattening. However, it does lie along the bright radio rim.

### 2.4. The *ASCA* Spectrum

The HXF and the ridge are embedded within the diffuse emission of IC 443 — at least in projection. Thus in order to determine the spectral properties of these features, one must first adequately characterize the “background” thermal emission. We therefore extracted a spectrum from the adjacent larger region shown in figure 3. We assume, based on the smoothness of the spectral hardness ratio map, that the spectrum of the diffuse emission does not vary appreciably in the neighborhood of the HXF; based on the previous X-ray observations the spectral variations in the diffuse emission would be most significant below 1 keV, outside the effective GIS band. To this “background” spectrum we fit an *ad hoc* thermal emission model, comprised of a thermal bremsstrahlung continuum and narrow Gaussians to represent the most prominent emission lines (the He $\alpha$  transitions of Ne, Mg, Si, S and Ar). Such *ad hoc* models have been used previously to model *ASCA* spectra

Table 2: Spectral Fits to Background Field and Hard X-ray Features

Model	Data Sets	$\chi^2$	$\chi^2_\nu$	$T_{\text{soft}}$ keV	$N_{\text{H}}$ $10^{22} \text{ cm}^{-2}$	Hard Component
1 Thermal <sup>a</sup>	Background	781	0.71	$0.89 \pm 0.03$	$0.12 \pm 0.03$	N/A
2 Thermal <sup>a</sup>	On HXF	793	0.73	$1.9 \pm 0.1$	0	N/A
3 Thermal <sup>b</sup>	On HXF	1407	1.28	0.89	$0.31 \pm 0.03$	N/A
4 Power-law <sup>c</sup> + Thermal <sup>b</sup>	On HXF	769	0.70	0.89	$0.18 \pm 0.03$	$\Gamma = 2.3 \pm 0.2$
5 Power-law + Thermal <sup>d</sup>	On HXF	766	0.70	$1.1_{-0.1}^{+0.3}$	0.12	$\Gamma = 2.4_{-0.4}^{+0.2}$
6 Hot Bremss + Thermal <sup>b</sup>	On HXF	763	0.70	0.89	$0.13 \pm 0.03$	$kT = 3.9_{-0.6}^{+1.7} \text{ keV}$
7 Thermal <sup>d</sup>	The Ridge	778	0.40	$0.74 \pm 0.08$	0.12	N/A
8 Power-law + Thermal <sup>b</sup>	The Ridge	755	0.39	0.89	$0^{<0.03}$	$\Gamma = 0.1 \pm 1.3$
9 Power-law + Thermal <sup>d</sup>	The Ridge	748	0.38	$0.54_{-0.16}^{+0.07}$	0.12	$\Gamma = 1.6_{-0.7}^{+1.4}$

Fits are to the energy range 0.5–12 keV

<sup>a</sup> Letting the scaling (GIS2 & GIS3), column density, temperature and line strengths vary

<sup>b</sup> We froze the line strengths and temperature to the off source (model #1) values, but fit the column density and scaling.

<sup>c</sup> The best-fit 5 keV flux density is  $(7 \pm 3) \times 10^{-13} \frac{\text{erg}}{\text{s cm}^2 \text{ keV}}$ .

<sup>d</sup> We froze the column density and line strengths to the off source (model #1) values, but fit the temperature and scaling.

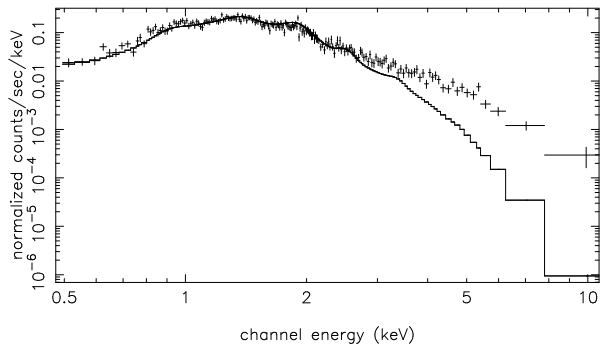


Fig. 5.— The *ASCA* GIS2 spectrum of the hard feature in IC 443 with the best-fit *ad hoc* thermal model. By adding a hard power law component to this model we reduce the combined GIS2 and GIS3  $\chi^2$  by  $\Delta\chi^2 = 640$ .

from other remnants (e.g. Miyata *et al.* 1994; Holt *et al.* 1994). The best fit model yields  $kT \sim 0.9$  keV, comparable with published temperatures for IC 443 (PSSW, WAHK). However, it is important not to over-interpret our thermal results, because we have made no attempt to distinguish the  $\text{He}\alpha$  transitions from weaker nearby spectral lines (including each element's corresponding H-like  $\text{Ly}\alpha$  transition) or to develop a physically self-consistent thermal model.

We next applied this same model to the GIS spectrum of the region containing the HXF (also shown in figure 3), allowing only the normalization to vary. As shown in table 2, this yields an unacceptable fit. As indicated in Fig. 5, the “background” model provides a good fit to the data below  $\sim 2$  keV, but there is a substantial flux excess at higher energies. An acceptable fit to the “on HXF” spectrum is obtained by adding a second continuum component. The current data do not allow us to distinguish between a power law with  $\Gamma = 2.3 \pm 0.2$  and thermal bremsstrahlung with  $kT = 3.9_{-0.6}^{+1.7}$  keV.

We also performed this same analysis using a smaller on-source region, tightly drawn around the HXF. However, this was less effective: because of the lack of thermal background counts, it is harder to spectrally distinguish the background from the non-thermal source emission. Nevertheless we measure a photon index of  $\Gamma = 2.2_{-0.4}^{+0.1}$ , using the technique described above.

We applied the same spectral analysis procedure as described above for the HXF to the hard ridge. Since the ridge is farther from the “background” region than the HXF (see Fig. 3) and we fit the thermal model using the AO-1 data, we were uncertain if it was appropriate to use the same background thermal model for both the HXF and the ridge. To test

this, we performed our analysis using both the AO-1 “background” region shown in Fig. 3 and one using PV phase data closer to the ridge. We do not detect any significant difference in the spectral index or flux of the hard ridge region as a function of the chosen background region.

Because of its larger extent and lower surface brightness, the ridge spectrum has lower signal to noise than the HXF. As with the HXF, fitting the spectrum with the background model yielded a clear excess above 2 keV. It was not possible, however, to constrain the spectral properties of the ridge’s hard component. While we have no evidence suggesting a different spectral form, we cannot eliminate the possibility that the hard emission from the ridge has a different origin.

The GIS spectral parameters for this region are similar to those obtained using the non-imaging (1°field of view) *Ginga* LAC. WAHK reported the presence of a hard component that was fit by a thermal model with  $kT=11^{+7.5}_{-2.0}$  keV (from their Fig. 3) or a power-law with photon index  $\Gamma = 2.2 \pm 0.13$ . Assuming a uniform surface brightness inside the shell and an absorbing column density of  $N_H = 10^{21.9} \text{ cm}^{-2}$ , WAHK found the total 2–20 keV emitted flux from IC 443 to be  $9 \times 10^{-11} \text{ erg cm}^{-2} \text{ s}^{-1}$ . As the total flux is dominated by the  $\sim 1$  keV thermal component, a comparison between the broad band *Ginga* flux and the GIS flux from the hard features is inappropriate. A more reasonable quantity to compare is the flux density at 7 keV, where the relative contribution of the  $\sim 1$  keV component is negligible. Using Figure 2 in WAHK, and assuming that the *Ginga* LAC has an effective area of  $3000 \text{ cm}^2$  and near unity quantum efficiency at 7 keV, we estimate the *Ginga* flux density at 7 keV to be  $20 \times 10^{-5} \text{ photons s}^{-1} \text{ keV}^{-1} \text{ cm}^{-2}$ . From the GIS data, we find the HXF flux density at 7 keV to be approximately  $4 \times 10^{-5} \text{ photons s}^{-1} \text{ keV}^{-1} \text{ cm}^{-2}$ , and the flux density of the portion of the hard ridge within the field of view to be about  $2 \times 10^{-5} \text{ photons s}^{-1} \text{ keV}^{-1} \text{ cm}^{-2}$ . Thus the detected flux in the hard regions seems to account for only 30% of the hard flux detected by *Ginga*, despite their prominence in the GIS images. Moreover, integration over the rest of the surface of the remnant contained in the GIS fields (about 90 percent of the total) yields a flux density of no more than  $4 \times 10^{-5} \text{ photons s}^{-1} \text{ keV}^{-1} \text{ cm}^{-2}$ , leaving a factor of two discrepancy between the GIS and *Ginga* 7 keV flux densities.

Two possible resolutions of this discrepancy are that there is significant hard flux from the small fraction of IC 443 unobserved by the GIS, or there is a calibration discrepancy between the GIS and *Ginga*. To check this latter possibility, we compare the broad band flux from all of IC 443 in the common 2–10 keV band. The 2–20 keV *Ginga* flux is  $9 \times 10^{-11} \text{ ergs cm}^{-2} \text{ s}^{-1}$  (WAHK). The 2–10 keV flux from IC 443 as measured by *HEAO1* A-2 is  $7 \pm 1 \times 10^{-11} \text{ ergs cm}^{-2} \text{ s}^{-1}$  (PSSW), consistent with the *Ginga* measurement. Integrating the 2–10 keV flux within the field of view of the two GIS pointings, we find  $5 \pm 1 \times 10^{-11} \text{ ergs cm}^{-2} \text{ s}^{-1}$ ; this represents 90 percent or more of the total flux from the remnant. The consistency of these numbers indicates that contribution of cross calibration uncertainties to the discrepancy is probably small, but could be as large as a factor of 2. Thus while it is possible that the GIS has observed all the regions in IC 443 producing hard flux, we cannot rule out the possibility that the unobserved portion of the IC 443 rim to the south and east of the ridge contribute significantly to the hard flux.

A key conclusion about the spatial distribution of the hard X-ray emission in IC 443, independent of a resolution of this discrepancy, is that the hard emission is highly localized. The flux density from the bulk of the remnant surface area is at most 40 percent of the total hard flux. This provides a strict upper limit on the luminosity of a hard thermal component, distributed throughout the remnant. WAHK inferred that IC 443 is a very young (1200 y) remnant based on their interpretation of the hard component as hot gas arising from a high velocity shock, and IC 443’s coincidence with the guest star of 837 A.D. Despite the restrictive limit we have placed on the flux of a hot thermal component, we nevertheless cannot rule out their conclusion about the age of IC 443. Moreover, high shock velocities may also be required to accelerate electrons to the relativistic energies required for the emission of X-ray synchrotron radiation, and WAHK’s historical evidence is naturally unaffected by our observations.

## 2.5. Pulsation Search

In order to search for periodicity from the unresolved HXF, we performed coherent fast Fourier transforms (FFTs) on the *ROSAT* HRI and *ASCA* events recorded from the region used for spectral analysis (after applying the standard barycenter corrections). All our results are consistent with a non-

periodic signal.

The temporal resolution of the GIS is 0.0625 s, so we cannot use the GIS data to search for a frequency faster than 8 Hz. On the other hand, the *ROSAT* HRI data have millisecond resolution. We therefore performed summed FFTs on the combined data set (*ROSAT* + *ASCA*) in the low frequency range 0.05–8 Hz, and only the *ROSAT* data in the high frequency range 10–1000 Hz. We find 99% confidence pulsed fraction upper limits of  $\sim 15\%$  and  $\sim 33\%$  in the low and high frequency ranges respectively.

### 3. Discussion

#### 3.1. Summary of Results

We have discovered an isolated hard X-ray emitting feature and a ridge of hard emission in the south-east of the SNR IC 443 using the *ASCA* GIS. The HXF's X-ray spectrum can be characterized by either a power law of energy spectral index  $\alpha=1.3\pm 0.2$  or thermal bremsstrahlung with  $kT=3.9^{+1.7}_{-0.6}$  keV; the ridge spectrum appears similar. The features can account for most of the hard X-ray flux from IC443 (§2.4). The core of the HXF is marginally resolved with the *ROSAT* HRI, but the low level surrounding emission extends about 10' along the radio-bright shell. (§2.2, fig. 4). It is spatially coincident with the  $\lambda\lambda 20$ –200 cm flat spectral ( $\alpha \approx 0.2$ ) region (G86; fig. 2), and in the general region of, but not uniquely coincident with, regions of cloud/shock interactions (DeNoyer, 1979; fig. 2). It is located outside the 95 percent confidence error circle of the nearby EGRET source (EHKS; fig. 2). No strong periodicity is observed from the feature, with a pulse fraction upper limit of 33% (§2.5), and there is no known pulsar near it.

#### 3.2. Origin of the Emission

We focus here on the origin of the emission from the HXF. Because of the uncertainty of the spectral parameters we know substantially less about the ridge. While some of our discussion below applies to all the emission (e.g. our conclusion that it is non-thermal), a more definitive understanding of the nature of the ridge emission (which could be different from that of the HXF) awaits a better quality X-ray spectrum.

The data suggest that the most likely mechanism for producing hard X-rays is synchrotron emission. Before addressing whether this emission arises from a

plerion or shock accelerated electrons, we first discuss our rationale for ruling out alternative mechanisms, including bremsstrahlung from a thermal and a non-thermal population of electrons, and inverse-Compton scattering.

**Thermal Bremsstrahlung** A thermal bremsstrahlung model provides an adequate fit to the *ASCA* and the *Ginga* spectra separately. The inferred temperatures are discrepant, however ( $\approx 15$  keV for *Ginga* versus  $\approx 4$  keV for *ASCA*). In contrast, a power law model yields the same photon index. If the 2–20 keV spectrum is better characterized by a power law, then the temperature obtained from a thermal model fit from each instrument would yield a temperature characteristic of the instrumental bandpass, which is exactly the case here. Thus, a thermal bremsstrahlung model is inconsistent with the *ASCA* and *GINGA* observations taken together.

**Inverse Compton** One possibility discussed by WAHK is that X-rays are produced by inverse-Compton scattering of infrared photons off electrons. Gaisser et al. (1996) found that an inverse-Compton component, scattering off the microwave background, would have a photon index of  $\Gamma=1.5$ . On the other hand, if the scattering photons were locally produced, one would expect the hard X-ray emission to arise from IR-bright regions. The localization of the hard X-ray emission a restricted region, the brightest part of which has no IR counterpart argues against an inverse-Compton origin.

**Accelerated Bremsstrahlung** It has been suggested that electrons accelerated in the shock to MeV energies may be responsible for the generation of hard X-rays via bremsstrahlung in supernova remnants (Sturner et al. 1995; Asvarov et al. 1990). The fact that the radio spectral index around the hard X-ray feature is flatter than elsewhere in IC 443 is strong evidence against this mechanism. If we assume that the same acceleration mechanism produces both the MeV and the GeV electrons (responsible for the radio emission), then there will be fewer MeV electrons in the hard region than elsewhere in the remnant. Thus, if this mechanism were operating efficiently, this region would be *dimmer* in hard X-rays than everywhere else in the remnant.

**Synchrotron Radiation** The most straightforward mechanism for producing a power law X-ray spectrum is synchrotron radiation. None of the observations contradict this interpretation; all are consistent with it. In particular, the fact that the radio spectrum of this region is flatter than elsewhere argues that at higher energies (including the X-ray band), the synchrotron flux will be enhanced over elsewhere in the SNR. In fact, as we show below, the physical size of the HXF corresponds well with the synchrotron loss time of X-ray producing electrons.

WAHK dismissed synchrotron emission as a likely model, because an acceleration mechanism efficient enough to accelerate electrons to  $\sim 10$  TeV seemed unlikely and they calculated synchrotron loss times to be less than the age of the SNR. Their dismissal was based on the assumption that the hard X-ray emission is spatially uniform; we now know from this *ASCA* observation that the hard emission arises primarily from localized regions.

X-ray synchrotron emission in a SNR can be produced by high energy electrons accelerated and interacting with a magnetic field in one of two locations: the magnetosphere of a pulsar (giving rise to a plerion) or the forward shock of a SNR. The observations support both interpretations to some extent, but more issues arise from the presence of a plerion than from an isolated region of intense shock acceleration.

The compact size of the hard X-ray feature is the primary evidence in favor of a plerionic interpretation. The lack of X-ray pulsations is not necessarily a problem: the upper limit on the pulsed fraction is higher than other pulsars like Vela (Pravdo et al. 1976). Nor is the existence of extended emission without an obvious embedded point source unprecedented: the SNR 3C 58 has a small extent, a power law spectrum and shows no pulsations, but is generally regarded as a plerion (Helfand et al. 1995).

Difficulties with the interpretation arise when trying to associate a plerion with IC 443. Wilson (1986) has shown that the median X-ray:radio ( $0.5\text{--}3.5$  keV)  $10^7\text{--}10^{11}$  Hz flux ratio for plerions is about 1, with a range from about 0.1–500. The flux ratio of the HXF is about 900, which would give it the highest known X-ray:radio flux ratio of any plerion.

Furthermore, if the feature is a plerion associated with the IC 443 shell it requires an extremely high

projected velocity of  $5,000 \left(\frac{d}{1.5 \text{ kpc}}\right) \left(\frac{\theta}{10'}\right) \left(\frac{t}{1000 \text{ yr}}\right)$  km s $^{-1}$ , for distance  $d$ , angular distance  $\theta$  from the explosion center, and age  $t$ . IC 443 is in a complex region of interstellar space, and the diffuse emission is thought to be the product of multiple supernova events (AA94). The proper motion problem is circumvented if the hard X-ray feature represents the site of the most recent explosion which we can take from Chinese records to have occurred in A.D. 837 (WAHK). If that were the case, then it is surprising that this explosion has apparently not affected the temperature or surface brightness distribution of the diffuse emission. The former suggests a more centrally located explosion; the latter an explosion in the northeastern quadrant of the SNR.

On the other hand, the presence around the hard feature of many interesting structures associated with collisions between the shock front and concentrations of material suggests the hard X-ray emission is related to them. In particular, shock/cloud collisions can locally enhance particle acceleration (JK93). We consider first whether shock acceleration is a plausible source of the hard X-rays, and then how the morphology of the feature might arise.

Dickel & Milne (1976) found Faraday rotation measures in IC 443 of about 200 rad m $^{-2}$  where the field is along the line of sight, and close to zero where it is perpendicular. Taking the density and path length measurements from the X-ray (PSSW), we estimate the magnetic field strength  $B$  to be:

$$B \approx 1.23 \times \left( \frac{200 \text{ rad m}^{-2}}{5 \text{ cm}^{-3} \times 0.1 \text{ pc}} \right) \approx 500 \mu\text{G} \quad (1)$$

The synchrotron photon/electron energy relation therefore can be written:

$$E_{\text{photon}} \approx 5 \text{ keV} \times \frac{B}{500 \mu\text{G}} \times \left( \frac{E_e}{20 \text{ TeV}} \right)^2, \quad (2)$$

where  $E_{\text{photon}}$  is the observed photon energy produced as synchrotron radiation from an electron at energy  $E_e$ . So while radio emission ( $E_{\text{photon}} \approx 10^{-9}$  keV) is produced by GeV electrons, production of 5 keV X-rays requires the presence of  $\sim 20$  TeV electrons.

In attempting to explain the non-thermal component dominating the X-ray emission from SN 1006 as synchrotron emission from highly relativistic electrons, Reynolds (1996) has shown that it is possible to accelerate electrons (and ions) in SNR shocks to energies exceeding 100 TeV. While his model is not strictly

applicable here, some aspects of it can be used to establish the plausibility of shock accelerated electrons as the source of the hard X-ray emission in IC 443.

In the simplest models, the synchrotron spectrum is expected to be a broken power law. The various break frequencies correspond to electron energies where two canonical times scales equate, such as the synchrotron loss time and the acceleration time scale. At each break, the spectral index increases by about 0.5. The electron diffusion time is also important in determining the steepening of the spectrum, but its influence is less straightforward to estimate.

In the IC 443 hard feature, the difference between the radio and the X-ray spectral index is approximately 1.1, suggesting the need for at least two spectral breaks between the bands. The time it takes for an electron of energy  $E$  to lose half its energy via synchrotron radiation in a magnetic field of strength  $B$  is given by:

$$\tau_{\text{loss}} = \left( \frac{500 \text{ }\mu\text{G}}{B} \right)^2 \left( \frac{20 \text{ TeV}}{E_e} \right) \times 2.5 \text{ years}, \quad (3)$$

which is approximately the light crossing time of the HXF. Using Equations 3 and 2, and assuming a SNR age between 1000 and 5000 yr (WAHK, AA94), we find that the break frequency where the synchrotron loss time becomes comparable to the age of the SNR occurs in the far infrared. Additionally, by assuming a shock velocity on the order of  $1000 \text{ km s}^{-1}$ , we find the break frequency associated with the equivalence between the acceleration and loss times is in the hard ultraviolet band. The frequencies at which these two spectral breaks occur supports the idea that the flat radio and the hard X-ray spectra are both produced by shock acceleration.

While Reynolds' (1996) formalism facilitates the plausibility argument above and is especially suggestive with regard to the ridge region, his models for producing X-rays from shock accelerated electrons from a large segment of the SNR shell clearly do not apply to the HXF in IC 443. A different mechanism must be operating there. Such a mechanism has been suggested by JK93.

Figure 2 shows BGBW's  $\text{H}_2$  image of shocked molecular gas. This shows that the molecular cloud has a clumpy ring structure exterior to the site of the supernova event. Dickman *et al.* (1992) found that if the ring is circular, it must be inclined  $\sim 51^\circ$  from the line of sight and have a diameter of  $\sim 9 \text{ pc}$ . Doppler shift information shows the southern edge of the ring

(near our HXF) expanding toward us, and the northern edge away – implying that the ring is now expanding at a deprojected velocity of  $25 \text{ km/s}$ . While, we agree with this picture in principle, we point out that to second order the ring is not circular; most noticeably there is a section of negative curvature surrounding the HXF (Fig. 2). It is this change of curvature that may create the HXF.

JK93 simulated cosmic-ray acceleration as shocks impact dense clouds – which is the case here. They found that after a shock/cloud impact, particle acceleration is significantly enhanced in the “tail shock” emanating from the cloud in the direction of shock propagation. Their results suggest that each clump in the molecular ring could produce enhanced shock acceleration in a long tail behind it. Because of the negative curvature of one section of the ring, the flow will be refracted, thereby “focusing” the enhanced shock acceleration at the hard X-ray feature where the tail shocks overlap. This interaction between these tail shocks will both increase the effective shock velocities and provide a complicated structure which will require further study.

The total hard flux from the diffuse emission along the shell (the ridge) is about half that from the HXF, but the ridge may extend out of the field of view. It corresponds to an arc bright in  $\text{H}_2$ , and radio continuum. While we cannot yet be certain that the emission is non-thermal, the higher ambient density as indicated by the infrared line emission argues that the temperature of shock-heated material should be lower than elsewhere in IC 443 – not higher. The arguments made above for the HXF against emission mechanisms other than synchrotron hold for the ridge region as well. While we withhold judgment until a higher quality spectrum can be obtained, we suggest that we are seeing evidence here as well for TeV electrons. Whether these arise from the JK93 mechanism or are more closely related to the forward shock is still an open question.

#### 4. Conclusion

In this paper we have presented evidence for a localized region of particle acceleration to electron energies over 20 TeV, within the shell type supernova remnant IC 443. Because of the unique positions of the hard X-ray feature and shocked clouds, we believe that the HXF is caused by the focusing of tail shocks around each molecular cloud, thus enhancing

particle acceleration in this location. In addition we have found a ridge of hard emission which is coincident with both the radio-synchrotron shell and shocked molecular gas, but whose spectral parameters are poorly constrained.

More observational and theoretical research is needed to fully understand this phenomenon. Multi-frequency and polarization observations with the VLA will allow us to both measure the feature's spectral index and look for other indicators of on-going particle acceleration. A deep single-dish radio observation of this area is necessary to verify that the HXF is indeed non-plerionic. The most important future observation will be to observe the full extent of the ridge and the shocked molecular gas with ASCA to better characterize the spectrum and image the full extent of the hard non-thermal emission.

On the theoretical side, this discovery provides a nice opportunity to model particle acceleration and cloud/shock interactions with significant observational constraints.

We thank the following people for contributing to these results: Richard Mushotzky for bringing the hard feature to our attention; Michael Burton for kindly providing his H<sub>2</sub> emission line image in digitized form; Steve Reynolds and Tom Jones for their insights into shock acceleration; Matthew Baring and Ocker de Jager for their thoughtful comments and suggestions.

## REFERENCES

Allen, G.E., et al., 1995, ApJ, 448, L25

Asaoka, I., & Aschenbach, B. 1994, A&A, 284, 573 (AA94)

Asvarov, A.I., Guseinov, O.H., Kasumov, F.K. & Dogel, V.A., 1990, A&A, 229, 196A

Axford, W.I., 1994, ApJS, 90, 937

Biermann, P.L., 1995, Space Sci. Rev., 74, 385

Blandford R.D. & Ostriker J.P., 1978, ApJ, 221, L29

Burton, M.G., Geballe, T.R., Brand, J.L. & Webster, A.S., 1988, MNRAS, 231, 617 (BGBW)

Burton, M.G., Hollenbach, D.J., Haas, M.R. & Erickson, E.F., 1990, ApJ, 355, 197

DeNoyer, L.K., 1979, ApJ, 232, L165

Dickel, J.R. & Milne, D.K., 1976, Aust. J. Phys., 29, 435

Dickman, R.L., Snell, R.L., Ziurys, L.M., Huang, Y.L., 1992, ApJ, 400, 203

Esposito, J.A., Hunter, S.D., Kanbach, G. & Sreekumar, P., 1996, ApJ, 461, 820 (EHKS)

Gaisser, T.K., Protheroe, R.J., Stanev, Todor, 1996, ApJ, *submitted*

Green, D.A., 1986, MNRAS, 221, 473 (G86)

Helfand, D.J., Becker, R.H. & White, R.L., 1995, ApJ, 453, 741

Holt, S.S., Gotthelf, E.V., Tsunemi, H. & Negoro, H., 1994, PASJ, 46, L151

Jones, T.W. & Kang, H., 1993, ApJ, 402, 560 (JK93)

Koyama, K., Petre, R., Gotthelf, E.V., Hwang, U., Matsuura, M., Ozaki, M. & Holt, S.S., Nature, 378, 255

Lasker, B.M., et al., 1990, AJ, 99, 2019

Miyata, E., Tsunemi, H., Pisarski, R. & Kissel, S.E., 1994, PASJ, 46, L101

Petre, R., Szymkowiak, A.E., Seward, F.D. & Willingale, R., 1988, ApJ, 335, 215 (PSSW)

Pravdo, S. H., Becker, R. H., Boldt, E. A., Holt, S. S., Rothschild, R. E., Serlemitsos, P. J. & Swank, J. H., 1976, ApJ, 208, L67

Reynolds, S.P., 1996, ApJ, 459, L13

Sturner, S.J. & Dermer, C.D., 1995, A&A, 293, L17

Sturner, S.J., Skibo, J.G., Dermer, C.D. & Mattox, J.R., 1995, BAAS, 187, #58.05

Sturner, S.J., Skibo, J.G. & Dermer, C.D., 1996, *in preparation*

Taylor, J.H., Manchester, R.N. & Lyne, A.G., 1993, ApJS, 88, 529

Wang et al. 1992, PASJ, 44, 303. (WAHK)

Wilson, A.S., 1986, ApJ, 302, 718